引用格式：LI Cunxia，LIU Yanghe，LI Zijian，et al. MTF Study of GBAII for Detecting Airglow 90～100 km above the Earth [J]. Acta Photonica Sinica，2022，51(3)：0301003
李存霞，刘洋河，李子健，等. GBAII探测地球上空90～100 km气辉MTF研究[J]. 光子学报，2022，51(3)：0301003

GBAII探测地球上空90～100 km气辉MTF研究

李存霞，刘洋河，李子健，惠宁菊，唐远河
（西安理工大学 理学院 应用物理系，西安 710048）

摘 要：分别利用He-Ne激光632.8 nm、O_2(0-1) 867.7 nm和O (^{1}S) 557.7 nm谱线作为光源，研究了地基气辉成像干涉仪的光学传递函数，给出了优化设计、理论计算和实际拍摄图片的MTF值。优化设计MTF的所有值均在0.3以上，部分视场MTF高于0.6；对557.7 nm和867.7 nm波长的气辉，理论计算的MTF分别为0.508和0.510；由室内外实验拍摄获取的GBAII成像干涉图得出的MTF值分别大于0.84、0.58、0.24，与国际著名的星载风成像干涉仪WINDII的0.35 MTF值相当。

关键词：地基气辉成像干涉仪；光学传递函数；干涉成像；气辉；光学仪器
中图分类号：O439 **文献标识码**：A **doi**：10.3788/gzxb20225103.0301003

0 引言

地球上空中高层大气(80～300 km)区域的微弱气辉、大气重力波、大气潮汐、夜光云、电离层闪电等现象大多出现在80～120 km的中间层和低热层(Mesosphere and Lower Thermosphere，MLT)区域，MLT区域是一个辐射、动力学和化学过程相互耦合的复杂区域。高空大气波的振幅在这里达到峰值，产生非线性相互作用和耗散，极大影响全球范围内大气的动量、能量、成分的分布和流动。MLT区域100 km附近电离层的等离子体电子分布出现峰值突变，这对通讯和广播造成严重影响，甚至讯号中断。MLT区域的金属离子层分布也严重影响卫星、飞行器的通讯信号。为了更多更好地了解诸如此类的自然现象，人们通常使用星载、机载、地基等主动和被动探测方式来获取大气的风速、温度、浓度等物理信息，这些观测方式中成本相对较低的是地基被动遥感探测方式[1-5]。国际上，地基的光谱气辉温度成像器(Spectral Airglow Temperature Imager，SATI)[6-7]和高分辨率多普勒成像仪(High Resolution Doppler Imager，HRDI)[8]均根据多原子分子振转谱线的强度差异，利用法布里珀罗干涉(Fabry - Pérot interferometer，FPI)滤光片的“转动谱线测温法”获取高层大气的温度，而星载的风成像干涉仪(Wind Imaging Interferometer，WINDII)[9]利用广角迈克尔逊干涉仪(Michelson Interferometer，MI)的“四强度法”探测高层大气温度和风速。中科院空间中心搭建了我国第一台FPI在国家天文台兴隆站进行观测[10]，西安交通大学利用广角MI对火星风场进行研究[11]。本课题组研制了一台揉合“转动谱线测温法”和“四强度法”原理于一体的地基气辉成像干涉仪(Ground-Based Airglow Imager Interferometer，GBAII)样机，成功探测了地球上空90～100 km的大气风速、温度[12-16]和体发射率[17]。GBAII使用地球上空98 km处的O(^{1}S) 557.7 nm单线气辉和94 km处的O_2(0-1)带867.7 nm附近的12条间距很小的谱线作为探测光源，将具备空间光谱扫描能力的窄带FPI的“转动谱线测温法”与具备视场展宽能力的广角MI“四强度测风法”相结合，从长时间曝光的气辉成像干涉图中获取地球上空90～100 km的大气风速、温度、体发射率等信息。

判断成像系统的像质优劣可用瑞利判据、中心点亮度、分辨率、点列图和光学传递函数(Modulation Transfer Function，MTF)等方式，而MTF是判断像质优劣的定量指标[18-20]。MTF是成像系统所成的像对

基金项目：国家自然科学基金(Nos. 41975040，61675165)，陕西省自然科学基础研究计划(Nos. 2020JM-444，2020JZ-46，2021JQ-469)
第一作者：李存霞(1978—)，女，讲师，博士，主要研究方向为高层大气风场地基探测技术。Email: licunxia@xaut.edu.cn
通讯作者：唐远河(1956—)，女，教授，博士，主要研究方向为高层大气风场和温度场探测原理与技术。Email: ltp1801@163.com
收稿日期：2021-09-29；**录用日期**：2021-11-16

被摄原物的还原比例，其值在0～1之间。因为GBAII是针对强度很弱的气辉既要成像还要发生干涉，其MTF就成为GBAII设计、研制和测试过程中一个非常重要的指标，本文针对GBAII的MTF开展研究。

1 GBAII优化设计的MTF

1.1 GBAII光学系统

GBAII的光学成像结构如图1所示，它由锥形镜收光系统、广角MI的相位调制系统、窄带干涉滤光片、CCD和3个透镜等5部分组成。图1顶部的锥形镜能保证光线的高通量，光线经锥形镜侧面反射，以一定角度入射到透镜1，再经MI、透镜2、透镜3后，出射的准直光束以一定离轴角进入干涉滤光片，通过干涉滤光片的光线由离轴角决定其空间光谱的分离，从CCD所拍摄气辉的成像干涉图来获取大气的温度和风速。实际光路中根据透镜焦距需要，GBAII分别用了3个透镜组合来等效图1所示的3个透镜，如图2所示，其中图2最右侧是激光光源，可以替换不同波长，用于室内定标等实验。GBAII的视场角为±6°，通过超广角、消色散、热补偿等条件优化出来的广角MI的基准光程差7.495 cm，所用CCD像素为512×512，单像素大小20 μm，GBAII选用峰值波长为557.7 nm、867.7 nm和630.0 nm窄带滤光片。

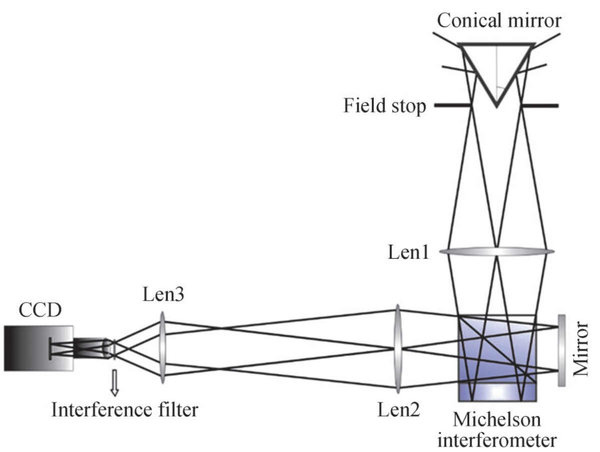

图1 GBAII光学系统示意图
Fig. 1 GBAII's simulate optical system

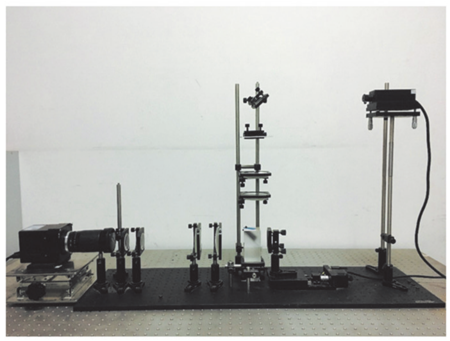

图2 GBAII光学系统实物图
Fig. 2 GBAII's optical components

1.2 GBAII优化设计的MTF

通过Code-V软件对图1所示的GBAII进行优化设计，得出GBAII的点列图如图3所示，采用4×4作为一个bin，0°视场时弥散斑直径约为60 μm，在2°～9.5°视场内，弥散斑控制在80～90 μm之间，极限分辨率为6.25 lp/mm。由于GBAII所用CCD的成像单元尺寸为20 μm，4个bin则为80 μm，这个弥散斑没有超过CCD的探测范围；点列图结果显示在0.4和0.7视场时弥散斑略有减小到40 μm左右，说明还有一定的慧差，全视场时大约100 μm，且有一定像散。

利用Code-V设计GBAII整个光学系统的MTF结果如图4所示，对波长为557.7 nm、630.0 nm和867.7 nm等3条气辉谱线，其MTF的所有值均在0.3以上，部分视场MTF高于0.6，但也看出全视场中的MTF子午分支和弧矢分支差别较大，主要由像散造成。如果采用2×2作为一个bin则极限分辨率为12.5 lp/mm，GBAII的MTF所有值均在0.3以上，部分视场在0.6以上。从这些MTF的设计结果可见GBAII满足较高的成像要求。

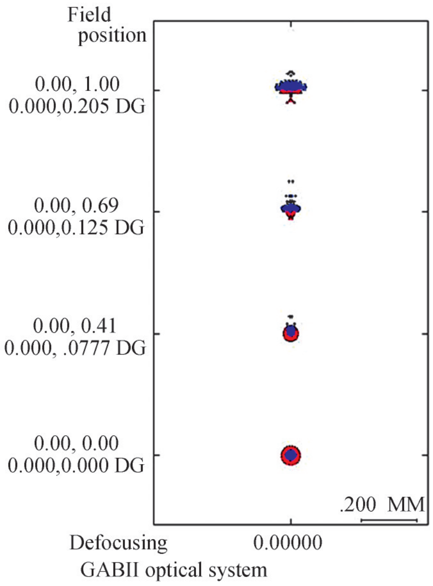

图 3　GBAII的点列图

Fig. 3　Spot diagram of GBAII

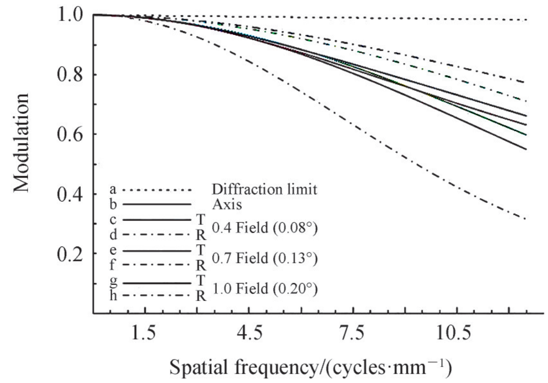

图 4　GBAII整个光学系统的MTF

Fig. 4　MTF diagram of GBAII

1.3　理论计算GBAII的MTF

根据傅里叶光学中线性光学系统调制传递函数的性质,GBAII的MTF的理论计算是图1所示的光学元件透镜1、MI、透镜2、透镜3、滤光片和CCD等6个部分的MTF之积。

$$\mathrm{MTF}(f)=\mathrm{MTF}_{\mathrm{len1}}(f)\cdot\mathrm{MTF}_{\mathrm{Michelson}}(f)\cdot\mathrm{MTF}_{\mathrm{len2}}(f)\cdot\mathrm{MTF}_{\mathrm{len3}}(f)\cdot\mathrm{MTF}_{\mathrm{filter}}(f)\cdot\mathrm{MTF}_{\mathrm{CCD}}(f) \tag{1}$$

以下分别计算式(1)中各部分的MTF值。对于透镜而言,虽然它的MTF与其孔径大小有关,孔径越大,透镜的MTF值就越大,透镜孔径的MTF因素与孔径的衍射效应有关,又与透镜的像差有关。一般说来,透镜的MTF值由商家给出,通常情况下为一个常数,取其为1。又由于该透镜的孔径与通光孔径大小相当,所以式(1)中将GBAII的3个透镜组的$\mathrm{MTF}_{\mathrm{len}}$均取值为1。

1.3.1　广角迈克尔逊干涉仪的MTF

GBAII的关键仪器之一是广角迈克尔逊干涉仪MI,GBAII采用中国K9玻璃且用大空气隙结构的MI。为了计算MI的MTF,需要把MI简化为正方形光瞳。根据边界条件,把GBAII入射光的x和y维度限定在$-a\leqslant x\leqslant a$,$-a\leqslant y\leqslant a$范围,设MI的入瞳函数为二维矩形函数

$$g(x,y)=\mathrm{rect}\left(\frac{x}{2a},\frac{y}{2a}\right)=\begin{cases}1 & (-a\leqslant x\leqslant a,\ -a\leqslant y\leqslant a)\\ 0 & (\mathrm{other})\end{cases} \tag{2}$$

根据衍射受限系统,成像的点扩散函数仅决定于系统的光瞳函数$g(x,y)$,且为光瞳函数的傅里叶变换;在相干照明下点扩散函数再进行一次傅里叶变换即为MTF。因为光瞳内MTF有值,光瞳外MTF为0,况且式(2)的二维矩形函数是对称的,所以只考虑一维情况下MI的归一化传递函数为

$$\mathrm{MTF}_{\mathrm{Michelson}}(f_x)=\mathrm{rect}\left(\frac{\lambda d_{i1}f_x}{2a}\right)=\begin{cases}1 & (0\leqslant\lambda d_{i1}f_x\leqslant 2a)\\ 0 & (\mathrm{other})\end{cases} \tag{3}$$

式中,λ是入射光的波长,d_{i1}是与图1中透镜组2的截止频率对应的焦距,f_x是空间频率。

1.3.2　干涉滤光片的MTF

设GBAII所用圆形干涉滤光片的底面中心为坐标原点,在横截面上取互相垂直的x,y方向,设滤光片厚度为1,当入射光沿主光轴方向到达滤光片时,则出射光瞳直径为$2b$的圆形光瞳函数为

$$p(x,y)=\mathrm{circ}\left(\frac{\sqrt{x^2+y^2}}{b}\right) \tag{4}$$

对式(4)进行傅里叶变换并归一化,得到滤光片的传递函数

$$\mathrm{MTF}_{\mathrm{circ}}=\left|\mathrm{FT}\{p(x,y)\}\right|=\left|\frac{J_1\left(2\pi b\lambda d_{i2}\sqrt{f_x{}^2+f_y{}^2}\right)}{b\lambda d_{i2}\sqrt{f_x{}^2+f_y{}^2}}\right|=\left|\frac{J_1(2\pi b\lambda d_{i2}\rho)}{b\lambda d_{i2}\rho}\right| \tag{5}$$

式中，$\rho=\sqrt{f_x{}^2+f_y{}^2}$，$d_{i2}$是与图1中透镜组3的截止频率对应的焦距，$J_1$是一阶贝塞尔函数。鉴于滤光片的光瞳函数具有圆域对称性，所以式(5)也只考虑一个方向的空间频率，于是干涉滤光片的一维归一化的传递函数为

$$\mathrm{MTF}_{\mathrm{filter}}=\left|\frac{J_1(2\pi b\lambda d_{i2}f_x)}{b\lambda d_{i2}f_x}\right| \tag{6}$$

1.3.3 CCD的MTF

CCD采样包含像元积分和离散抽样两过程，其MTF是这两部分之积。假设光敏面CCD的单个像素元尺寸为$w\times w$，则单个像元脉冲响应函数可表示为

$$l(x,y)=\mathrm{rect}\left(\frac{x}{w},\frac{y}{w}\right) \tag{7}$$

将式(7)进行傅里叶变换并归一化，得到CCD单个像素元的传递函数

$$\mathrm{MTF}_{\mathrm{ccd}}=\left|\mathrm{FT}\{l(x,y)\}\right|=\left|\mathrm{sinc}(wf_x,wf_y)\right| \tag{8}$$

鉴于CCD成像时还需在CCD像面上抽样采样，假设x,y方向的采样间距均为l，采样函数为

$$\mathrm{Samp}(x,y)=\mathrm{rect}\left(\frac{x}{l},\frac{y}{l}\right) \tag{9}$$

将式(9)进行傅里叶变换并归一化，得到采样的传递函数

$$\mathrm{MTF}_{\mathrm{samp}}=\mathrm{FT}\{\mathrm{Samp}(x,y)\}=\left|\mathrm{sinc}(lf_x,lf_y)\right| \tag{10}$$

因此，CCD的$\mathrm{MTF}_{\mathrm{CCD}}$是CCD单像素元的$\mathrm{MTF}_{\mathrm{ccd}}$与采样$\mathrm{MTF}_{\mathrm{samp}}$之积

$$\mathrm{MTF}_{\mathrm{CCD}}=\mathrm{MTF}_{\mathrm{ccd}}\cdot\mathrm{MTF}_{\mathrm{samp}}=\left|\mathrm{sinc}(wf_x,wf_y)\right|\cdot\left|\mathrm{sinc}(lf_x,lf_y)\right| \tag{11}$$

1.3.4 GBAII的计算MTF

综合式(1)、(3)、(5)和(11)，由于MI矩形、FPI圆形函数都具对称性，空间频率$f_x=f_y=f$，将二维MTF简化为一维来计算，则GBAII的MTF表达式为

$$\mathrm{MTF}(f)=\mathrm{rect}\left(\frac{\lambda d_{i1}f}{2a}\right)\cdot\left|\frac{J_1(2\pi b\lambda d_{i2}f)}{b\lambda d_{i2}f}\right|\cdot\left|\mathrm{sinc}(wf)\right|\cdot\left|\mathrm{sinc}(lf)\right| \tag{12}$$

根据超广角、消色散、热补偿条件优化出来的广角GBAII的相关结构和尺寸[5]，将$a=25$ mm，$d_{i1}=18.89$ cm，$b=20$ mm，$d_{i2}=1$ mm，$w=0.02$ mm，$l=0.0146$ mm，$\lambda_1=557.7$ nm，$\lambda_2=867.7$ nm带入式(12)，画出GBAII的MTF曲线如图5所示。从图5可见，对557.7 nm和867.7 nm波长的气辉，MTF分别为0.508和0.510，对应奈奎斯特频率分别为20 lp/mm和16 lp/mm。成像系统的MTF值越高，表明该系统的分辨率越高。对于我们研制的GBAII，在低频处MTF值大于0.51，大于WINDII的0.35 MTF[10]。

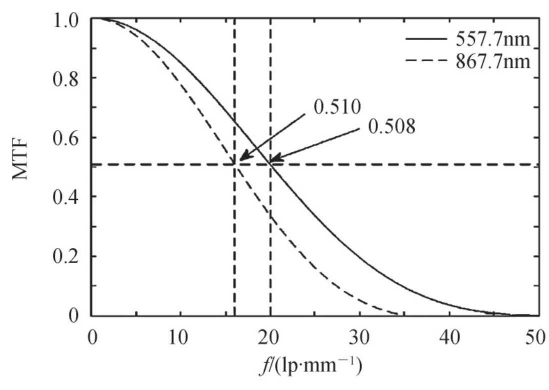

图5 GBAII的MTF计算值

Fig. 5 Computational MTF curve of GBAII

2　实验及讨论

GBAII样机研制成功后进行了多次拍摄。图6(a)是利用GBAII和波长632.8 nm的He-Ne激光器在实验室拍摄得到的干涉图,图6(b)是利用GBAII在西安理工大学教9楼顶(N34°13′22.21″, E108°59′38.14″)拍摄地球上空94 km的O_2(0-1) 867.7 nm气辉的成像干涉图(图中白点是星星),图6(c)是利用GBAII在临潼仁宗庙(N34°19′56.57′′,E109°16′53′′)山顶拍摄地球上空98 km的O(^{1}S) 557.7 nm气辉的成像干涉图。

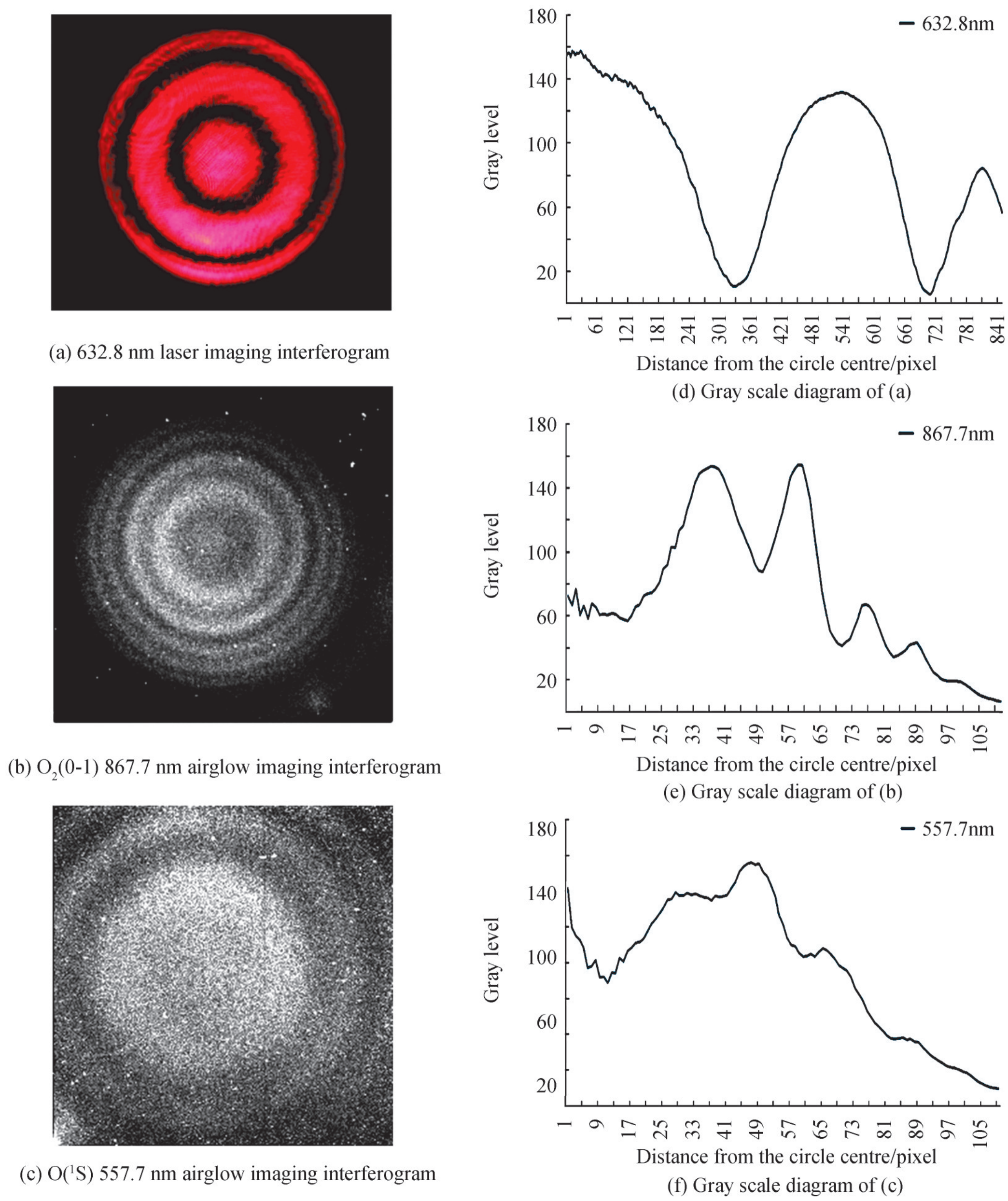

图6　GBAII拍摄所得的成像干涉图和其灰度值,所用光源分别是632.8 nm激光, 867.7 nm气辉, 557.7 nm气辉

Fig.6　Imaging interference fringes and gray level distribution of GBAII. The light sources used in the interferogram are 632.8 nm laser, O_2(0-1) 867.7 nm airglow and O(^{1}S) 557.7 nm airglow respectively

为了从实验图像中得到GBAII的MTF,先计算干涉条纹的对比度。对比度表征干涉图像的清晰程度,其值为

$$V=\frac{I_{\max}-I_{\min}}{I_{\max}+I_{\min}} \tag{13}$$

式中，I_{max}和I_{min}为干涉条纹的最大和最小强度。通过GBAII拍摄图6(a)～(c)所示的成像干涉图像，利用C++编程逐点读取图像的灰度值，对应得到干涉条纹灰度值的分布如图6(d)～(f)所示，其中横坐标是干涉圆环上各点到圆心的距离，纵坐标是灰度值；根据式(13)，取图6(d)的第二个亮环与第二个暗环的灰度值，得到图6(a)的最大对比度为0.84；取图6(e)的第二个暗环与第二个亮环的灰度值，得到图6(b)的对比度为0.58；取图6(f)的第二个亮环与第三个亮环的灰度值，得到图6(c)的对比度为0.24。

鉴于成像系统的MTF等于像的对比度(V_i)除以物的对比度(V_o)：$MTF(f)=V_i/V_o$。事实上被摄物体的对比度V_o不等于1而小于1，所以对632.8 nm激光、867.7 nm和557.7 nm气辉，用GBAII拍摄得到的成像干涉图的MTF实验值分别大于0.84、0.58和0.24。

由于GBAII观测的是地球上空90～100 km的气辉扩展光源，从实验的MTF值来看，GBAII对双原子O_2分子的振转谱线的成像效果优于单原子O气辉。$O(^1S)$ 557.7 nm和$O_2(0\text{-}1)$ 867.7 nm气辉的强度都很低，GBAII在地面上需要通过长时间曝光方式获得气辉的成像干涉条纹。从结果上来看，GBAII室外实验得到两条气辉谱线的MTF结果与实验室632.8 nm氦氖激光的MTF有一定差距，可以通过后期GBAII的进一步优化来改进。

3 结论

地基气辉成像干涉仪GBAII用于探测地球上空90～100 km处的大气风速和温度。本文研究了GBAII成像系统的MTF。通过Code-V对GBAII系统的优化设计结构表明，奈奎斯特频率处子午方向的MTF为0.43，全视场弧矢方向的MTF为0.18，中心视场处MTF值为0.31；对波长为557.7 nm、630.0 nm和867.7 nm等3条气辉谱线，其MTF的所有值均在0.3以上，部分视场MTF高于0.6。通过傅里叶光学规律对GBAII的MTF进行理论计算后，得出GBAII整体系统的MTF表达式，代入GBAII在超广角、消色散、热补偿条件下的相关参数，对波长为867.7 nm和557.7 nm的气辉，在奈奎斯特频率处的MTF分别为0.510和0.508；在实验室内外分别利用632.8 nm He-Ne激光器、$O_2(0\text{-}1)$ 867.7 nm和$O(^1S)$ 557.7 nm气辉作为光源，拍摄得到GBAII的成像干涉图，得到实验MTF值分别大于0.84、0.58、0.24。

可以看出GBAII优化设计、理论计算和实际拍摄图片的MTF值有一定偏差，用激光作为光源GBAII的实验值MTF值最大，对557.7 nm气辉谱线的实验MTF稍小，软件优化MTF值居中。总体来看，GBAII的MTF值与WINDII的0.35 MTF相当。通过本文研究GBAII的MTF值可见，GBAII对双原子O_2分子的振转谱线成像效果好于单原子O气辉，以后要开发GBAII用于多原子的气辉测试，改进对单原子气辉谱线的成像效果。这些研究为GBAII进一步探测高层大气风速、温度、体发射率等物理量提供了理论保证。

参考文献

[1] RAHNAMA P, GAULT W, IMCDADE, et al. Onboard calibration and monitoring for the SWIFT instrument[J]. Measurement Science and Technology, 2012, 23(10): 105801.

[2] LIU S, SHEPHERD G G, CHEN Y, et al. WINDII observations and WACCM-X simulations of high-latitude winds under different solar radio flux and geomagnetic disturbance conditions[J]. Journal of Geophysical Research: Space Physics, 2019, 124(7):6087-6096.

[3] NICIEJEWSKI R, WU Q, SKINNER W, et al. TIMED doppler interferometer on the thermosphere ionosphere mesosphere energetics and dynamics satellite: data product overview[J]. Journal of Geophysical Research, 2006, 111 (A11S90): 1-20.

[4] VARGAS F. Uncertainties in gravity wave parameters, momentum fluxes and flux divergences estimated from multi-layer measurements of mesospheric nightglow layers[J]. Advances in Space Research, 2019, 63(2): 967-985.

[5] SOLHEIM B, BROWN, S, SIORIS C, etal: SWIFT-DASH: spatial heterodyne spectroscopy approach to stratospheric wind and ozone measurement[J]. Atmosphere-Ocean, 2015, 53 (1): 50-57.

[6] SARGOYTCHEV S I, BROWN S, SOLHEIM B H, etal. Spectral Airglow Temperature Imager (SATI): a ground-based instrument for the monitoring of mesosphere temperature[J]. Applied Physics, 2004, 43(30): 5712-5721.

[7] CHO Y M, SHEPHERD M G , SHEPHERD G G . Wave perturbations in the MLT at high northern latitudes in winter, observed by two SATI instruments[J]. Advances in Space Research, 2010, 45(1): 45-55.

[8] HAYS, P B, ABREU V J, DOBBS M E, et al. The high-resolution Doppler imager on the upper atmosphere research satellite[J]. Journal of Geophysical Research Atmospheres, 1993, 98(D6): 10713-10723.

[9] SHEPHERD G G, THULLIER G, GAULT W A, et al. WIND Ⅱ the wind imaging interferometer on the upper

atmosphere research satellite[J]. Journal of Geophysical Research, 1993, 98(D6): 10725-10750.
[10] YU Tao, XIA Chunliang, ZUO Xiaomin, et al. A comparison of mesospheric and low-thermospheric winds measured by Fabry Perot interferometer and Meteor Radar over Center China[J]. Journal of Geophysical Research Space Physics, 2016, 121(10): 10037-10051.
[11] RONG P, ZHANG C, WARD W E, et al. Compensation optimization for a static Mars wind imaging Michelson interferometer[J]. Optics and Lasers in Engineering, 2021,142(3): 106589.
[12] TANG Yuanhe, CUI Jin, GAO Haiyanget al. Calibrations of ground based airglow imaging interferometer for the upper atmospheric wind field measurement[J]. Acta Physica Sinica, 2017, 66(13): 65-74.
唐远河，崔进，郜海阳，等. 地基气辉成像干涉仪探测高层大气风场的定标研究[J]. 物理学报，2017, 66(13): 65-74.
[13] GAO Haiyang, TANG Yuanhe, HUA Dengxin, et al. Ground-based airglow imaging interferometer. Part 1: instrument and observation[J]. Applied Optics, 2013, 52(36): 8650-8660.
[14] TANG Yuanhe, DUAN Xiaodong, GAO Haiyang, et al. Ground-based airglow imaging interferometer. Part 2: forward model and inverse method[J]. Applied Optics, 2014, 53(11): 2273-2282.
[15] GAO Haiyang, TANG Yuanhe, HUA Dengxin, et al. Study on the wide-angle Michelson interferometer with large air gap[J]. Applied Optics, 2011, 50(29): 5655-5661.
[16] TANG Yuanhe, YANG Rui, GAO Haiyang, et al. Improving the atmospheric wind speed measured accuracy by the ground-based airglow imaging interferometer[C]. Proceedings of SPIE, 2017, 10256: 642-651.
[17] TANG Yuanhe, SUN Peng, GAO Haiyang, et al. Simulation and observation for volume emission rates emitted from O_2 (0-1) and $O(^1S)$ nightglow at northwest china[J]. Applied Optics, 2019, 84(4): 1093-1100.
[18] ZHENG Zhizhong, YANG Zhong, XIU Liancun, et al. Design of a SWIR offner imaging spectrometer[J]. Spectroscopy and Spectral Analysis, 2017, 37(7): 2267-2272.
郑志忠，杨忠，修连存，等. 一种Offner型小型短波红外成像光谱仪[J]. 光谱学与光谱分析，2017, 37(7): 2267-2272.
[19] SHI Dalian, FENG Yutao, ZHANG Geng, et al. Research on the calibration and data retrieval of the wind field measurement Fabry-Perot interferometer[J]. Acta Photonica Sinica, 2015, 44(8): 21-26.
石大莲，冯玉涛，张耿，等. 风场探测Fabry-Perot干涉仪定标与反演算法研究[J]. 光子学报，2015, 44(8): 21-26.
[20] KANG Jiqiang, CHENG Xuemin, HAO Qun. Two demensional modulation transfer function and its application in wavefront aberration detection[J]. Acta Photonica Sinica, 2014, 43(12): 131-137.
康吉强，程雪岷，郝群. 二维调制传递函数及其在波前差检测方面的应用[J]. 光子学报，2014, 43(12): 131-137.

MTF Study of GBAII for Detecting Airglow 90~100 km above the Earth

LI Cunxia, LIU Yanghe, LI Zijian, XI Ningju, TANG Yuanhe
(*Department of Physics, School of Science, Xi'an University of Technology, Xi'an* 710048, *China*)

Abstract: Ground-Based Airglow Imaging Interferometer (GBAII) is a ground-based wind field detection prototype developed by our research group that integrates the principles of "rotational spectral line temperature measurement" and "four-intensity method". The imaging interferogram of airglow 90～100 km above the earth can be obtained by taking long time exposure of 200 s. Then the information of atmospheric wind speed, temperature and volume emissivity over the Earth can be obtained from the imaging interference fringe. Modulation Transfer Function (MTF) is a very important index in the design, development and testing of ground-based airglow imaging interferometer GBAII, which can characterize the imaging quality of GBAII. In this paper, the modulation transfer function of ground-based airglow imaging interferometer is studied. By using He-Ne laser wavelength of 632.8 nm, O_2(0-1) 867.7 nm and $O(^1S)$ 557.7 nm as light sources, the MTF values of the optimized design, theoretical calculation and actual images are given. Firstly, the optical imaging structure of GBAII consists of five parts: a tapered mirror light receiving system, a wide-angle MI phase modulation system, a narrowband interference filter, a CCD and three lenses. The optical structure of GBAII is optimized by Code V, and the point sequence diagram of GBAII was obtained. 4×4 was used as a bin, and the diameter of dispersion spot was about 60 μm at 0° field of view, and 80～90 μm at 2°～9.5° field of view, and the limit resolution was 6.25 lp/mm. For the three airglow lines with wavelength 557.7 nm, 630.0 nm and 867.7 nm, all the MTF values are above 0.3, and some of the MTF values are higher than 0.6. However, it can also be seen that the MTF meridional branch and sagittal branch differ greatly in the full field of view, mainly caused by astigmatism. Secondly, according to Fourier optical theory, the MTF expression of GBAII optical system is obtained by calculating the MTF of wide-angle Michelson interferometer, interference filter and CCD. The MTF curve of GBAII is given by substituting the MTF expression of GBAII into the relevant structure and size of GBAII optimized by ultra-wide Angle, thermal compensation and achromatic conditions. For airglow wavelengths at 557.7 nm and 867.7 nm, the MTF value is 0.508 and 0.510, corresponding to Nyquist frequencies of 20 lp/mm and 16 lp/mm, respectively. For the GBAII developed by our researcher group, the MTF value is greater than 0.51 at low frequency, which is greater than 0.35 MTF of international famous wind imaging interferometer WINDII. Thirdly, in order to obtain the experimental MTF value of GBAII, it is necessary to take imaging interferogram through GBAII first, and use software to read gray value of image point by point to calculate contrast of interference fringes. The MTF of GBAII imaging system is equal to the contrast of the image divided by the contrast of the object, where, the contrast of the subject is not equal to but less than 1. He-Ne laser spectrum line of 632.8 nm, O_2(0-1) 867.7 nm and O (^{1}S) 557.7 nm were used as light sources respectively to obtain the indoor and outdoor imaging interferogram of GBAII. The experimental MTF of different wavelengths was obtained according to contrast of imaging interferogram. The MTF value of GBAII is greater than 0.8, 0.58 and 0.24 at the wavelength of 632.8 nm laser, O_2(0-1) 867.7 nm and O(^{1}S) 557.7 nm airglow, respectively. Based on the MTF value of GBAII studied in this paper, the experimental MTF values show that GBAII has better imaging effect on the vibration spectra of diatomic O_2 molecules than that of single atomic O airglow. Since the intensity of O(^{1}S) 557.7 nm and O_2(0-1) 867.7 nm airglow is very low, the imaging interference fringes of GBAII airglow need to be obtained by long time exposure on the ground. In terms of the results, the MTF results of the two airglow spectra obtained by GBAII outdoor experiment have a certain gap with that of the laboratory 632.8 nm He-Ne laser, which can be improved by further optimization of GBAII later. It can be seen from the above results that the MTF value of GBAII optimized design, theoretical calculation and actual image has a certain deviation. When laser is used as the light source, the experimental MTF value of GBAII is the largest, and the experimental MTF value of 557.7 nm airglow spectrum line is slightly smaller, and the MTF value of software optimization is in the middle. Overall, the MTF result of GBAII theory and experiment is better than 0.35 MTF of WINDII. The study of MTF of GBAII can provide technical basis for GBAII to successfully detect atmospheric wind field parameters. The research results can provide accurate technical basis for GBAII to successfully detect physical quantities such as wind speed, temperature and volume emissivity in the upper atmosphere, and also lay a theoretical and experimental foundation for the development of similar instruments in China.

Key words: Ground-based airglow imager interferometer; Modulation transfer function; Interferometric imaging; Airglow; Optical instrument

OCIS Codes: 010.1290; 080.2740; 110.3175; 120.4570; 220.2740

Foundation item: National Natural Science Foundation of China (Nos. 41975040, 61675165), Natural Science Basic Research Program of Shaanxi(Nos. 2020JM-444, 2020JZ-46, 2021JQ-469)